EXTRACTING DISTORTED GRID POINTS FOR COMPENSATION OF LENS RADIAL NONLINEARITIES

Artur Nowakowski, Władysław Skarbek

Institute of Radioelectronics, Warsaw University of Technology
Pl. Politechniki 1, 00-661, Warszawa, Poland
phone: + (48) 228253929, fax: + (48) 228253769, email: A.Nowakowski@ire.pw.edu.pl
web: www.ire.pw.edu.pl

ABSTRACT

A novel method for extracting distorted grid points for compensation of lens radial nonlinearities is presented. It is based on identification of homographic transformation using single image of dense planar chessboard pattern. Undistorted grid image is determined from the central part of the grid and used to find the radial distortion model by linear least square method (LSM). The model is used for dense compensation by bilinear interpolation.

1. INTRODUCTION

Optical lens distortion in contemporary off-the-shelf camera is a significant problem for low cost vision systems. It results in image point displacement of unacceptable size for applications. Therefore, systems using image based measurements, like 3D reconstruction systems, need robust distortion compensation methods.

The dominant optical distortion is of radial type which is visible as barrel or pincushion effect.

Many techniques for radial distortion modelling and compensation were published. The method presented in this paper determines values of radial model parameters and detects the distortion centre based on determined calibration points coordinates from a single image of the planar pattern. It presents a new fast approach to distortion centre estimation and results in high accuracy of compensation. It solves perspective problem by estimation of homographic matrix. Therefore, no special alignment of a camera with regard to the chessboard plane is needed.

2. SYSTEM DESCRIPTION

2.1 Assumptions

The method determines radial model parameters and localises distortion centre based on single image of planar chessboard pattern. The identified parameters are used to compensate an image.

Corners of chessboard squares are used as the calibration points. In order to assure the correct localisation of them, the distance between neighbouring points should be at least ten pixels and homogenous light condition should be ensured. It is not required to align the chessboard perpendicular to the optical axis of camera which is not easy task. However, in order to achieve high accuracy of results it is important to assure as much of calibration points as possible, which means that chessboard orientation should be close to perpendicular when the camera obscura model can be assumed.

We use precise radial distortion model, which defines distorted pixel coordinates as follows:

$$\tilde{p} = d(p) = p_0 + (p - p_0)[1 + d_1 \| p - p_0 \| + d_2 \| p - p_0 \|^2 + d_3 \| p - p_0 \|^3 + d_4 \| p - p_0 \|^4], \quad (1)$$

where $p \in R^{2\times 1}$ are undistorted pixel coordinates, $p_0 \in R^{2\times 1}$ are the co-ordinates of distortion centre and d_1, d_2, d_3, $d_4 \in R$ are model parameters. Notice that we use the *distortion model* rather than the *compensation model*. Paradoxically, having the distortion model makes the dense compensation for large images more efficient.

It is observed that in the centre of defined model the distortion is minimal. Therefore, we assume that distortion is negligible in the neighbourhood of image centre (model centre) and calibration points localised there are called as "good" ones, while the rest of calibration points are called as "bad" ones.

Considering the mentioned assumptions, the system realises the following steps:

- calibration points localisation with subpixel accuracy;
- localisation of distortion centre using calibration points**;**
- estimation of radial distortion parameters values;
- distortion compensation by obtained model.

2.2 Calibration points localisation

2.2.1 Edge Detection

To image of chessboard pattern, which fulfils conditions introduced in previous section, a noise removal is applied using Gaussian masks. Next, Canny algorithm for edge detection is employed [13]. For gradient computation Sobel masks are used [14]. The hysteresis (optional) step of Canny algorithm is not necessary if close to homogenous light condition are provided. If such condition can not be assured, the fast implementation of thresholding hysteresis can be employed [14].

Using the gradient orientation, the set of edge pixels is divided into two sets containing pixels with horizontal or vertical gradient orientation.

2.2.2 Calibration Points Rough Localisation

Next, rough co-ordinates of grid intersections are found. For this purpose the popular Harris filters can be used. However, instead of that we propose method of neighbourhood analysis, which does not need SVD computation. It uses mask shown in Fig. 1a. It is checked, for the current pixel, if there is at least one edge pixel having horizontal gradient orientation in top and bottom fields signed as H, respectively and if there is no edge pixel with vertical gradient orientation in any of field signed as H. Adequate conditions are checked for V-type fields. If they all are fulfilled, the actual pixel co-ordinates are the candidate for rough estimation of calibration point localisation. It is worth saying, that radius of neighbourhood analysis r (the distance between central point and H-type or V-type fields) was found experimentally and can be changed according to data characteristic. If two of found candidates are localised within a distance equal or smaller than r=2, only this one from them is promoted, for which neighbourhood analysis detected the higher number of edge pixels with horizontal

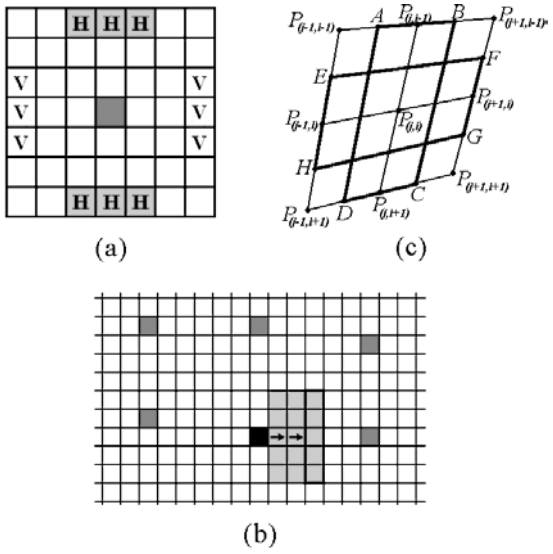

Figure 1 – Calibration points localisation: (a) - neighbourhood analysis with radius r=3 for rough localisation of calibration point, (b) - searching for right neighbour $P_{(0,1)}$ of point $P_{(0,0)}$, (c) - neighbourhoods of $p_{(j,i)}$ for PCA analysis

gradient orientation in H-type fields and with vertical gradient orientation in V-type fields. The other candidate is eliminated.

2.2.3 Indexing of Calibration Points Rough Localisations

Localised calibration points are indexed then. Firstly, calibration point, which is localised at the smallest distance to image centre is indexed as $p_{(0.0)}$. Next, its right neighbour is founded using iterative function on image with calibration points. During every iteration vertical searching window is moved one pixel right starting from calibration point indexed as $p_{(0,0)}$ (Fig. 1b). This process is continued until the first calibration point appears in the window. This point is indexed as $p_{(1,0)}$. Adequately, the function finds left $p_{(-1,0)}$, up $p_{(0,-1)}$ and bottom neighbour $p_{(0,1)}$. Next, function seeks for points $p_{(j,0)}$, for j=2,3,4,… Searching for $p_{(j,0)}$ point is made in a window with certain size. Localisation of a centre of the window is calculated as a sum of co-ordinates of calibration point $p_{(j,0)}$ and actual displacement vector between localisation of point $p_{(j,0)}$ and $p_{(j-1,0)}$. Thus, searching function is adjusted to local character of distortion. In case of point $p_{(j,0)}$ is not localised, the searching is proceeded: the searching window is moved by actual displacement vector and seeking next calibration points is made. For every found point $p_{(j,0)}$, j=0,1,2,3,4,… searching for points $p_{(j,i)}$ is made, firstly for i=1,2,… and then for i=-1,-2,… After such searching is finished, points $p_{(j,i)}$, j=-1,-2,.., i=…,-2,-1,0,1,2,… are indexed.

2.2.4 Calibration Points Exact Localisation

Having indexed rough positions of calibration points, the next step is to determine exact co-ordinates of them. Considering the fact, that image is nonlinearly distorted, methods determining intersections of global straight lines in image such as [15] cannot be applied. The method analysing local neighbourhood of rough localisation of calibration point was designed and used. In such neighbourhood, distortion influence is negligible and line can be considered as straight. Intersection of two of grid lines found using PCA in the neighbourhood leads to obtain co-ordinates of a calibration point with sub-pixel accuracy. For vertical line the neighbourhood of point $p_{(j,i)}$ is defined as an interior of tetragon ABCD (Fig. 1c), where A is geometrical centre of segment $p_{(j-1,i-1)}p_{(j,i-1)}$, and B, C, D are respectively geometrical centres of segments $p_{(j,i-1)}$, $p_{(j+1,i-1)}$, $p_{(j,i+1)}p_{(j+1,i+1)}$, $p_{(j-1,i+1)}p_{(j,i+1)}$. All of edge pixels having horizontal gradient orientation which are in the neighbourhood are used in PCA [16] in order to determine parameters of the best fitted line. Solution for PCA is found using SVD computation [17]. In adequate way horizontal line is found in tetragon EFGH. Intersection of horizontal and vertical line is an exact localisation of calibration point.

2.3 Distortion parameters estimation

Modelling of optical distortion is based on analysis of transformation of ideal planar grid of calibration points P_i, i=1,…,n, into image points p_i, which were localised and indexed. This transformation can be divided into two steps: perspective projection of calibration points P_i onto an image plane:

$$p_i \equiv MP_i, \qquad i = 1, \cdots, n, \tag{2}$$

and radial distortion of points co-ordinates on image plane according to (1):

$$\tilde{p}_i = d(p_i), \qquad i = 1, \cdots, n. \tag{3}$$

Calibration points are coplanar, therefore only 2D version of projection matrix has to be estimated, i.e. the homographic matrix H:

$$p_i \equiv HP_i, \qquad i = 1, \cdots, n. \tag{4}$$

2.3.1 Homographic Matrix Estimation

Perspective projection of chessboard plane onto image plane is determined by the unknown eight elements of the homographic matrix $H=[h_{ij}]$, $H \in R^{3\times3}$, $h_{33}=1$. They determine a transformation of point $P(X,Y)$ into image point $p(x,y)$ in homogenous co-ordinates:

$$HP \equiv p \quad \leftrightarrow \quad \frac{h_{11}X + h_{12}Y + h_{13}}{h_{31}X + h_{32}Y + 1} = x, \qquad \frac{h_{21}X + h_{22}Y + h_{23}}{h_{31}X + h_{32}Y + 1} = y. \tag{5}$$

Rewriting the equations we get their linear form for central points which can be considered as undistorted (good points):

$$\begin{aligned} &h_{11}X_i + h_{12}Y_i + h_{13} = h_{31}x_iX_i + h_{32}x_iY_i + x_i, \\ &h_{21}X_i + h_{22}Y_i + h_{23} = h_{31}y_iX_i + h_{32}y_iY_i + y_i, \\ &i = 1, \cdots, n_{good}. \end{aligned} \tag{6}$$

The values of h_{ij} are obtained by the linear Least Square Method (LSM). According to (1) the distortion size near the distortion centre is minimal. Therefore, we assume that the distortion is negligible for the calibration points around the distortion centre. We call such points as "good" ones and substitute them to (6) getting by LSM:

$$h_{opt} = \arg\min_h \|hA - b\|^2, \tag{7}$$

where A is $8\times 2n_{good}$ real matrix:

$$A = \begin{bmatrix} X_1 & \cdots & X_{n_{good}} & 0 & \cdots & 0 \\ Y_1 & \cdots & Y_{n_{good}} & 0 & \cdots & 0 \\ 1 & \cdots & 1 & 0 & \cdots & 0 \\ 0 & \cdots & 0 & X_1 & \cdots & X_{n_{good}} \\ 0 & \cdots & 0 & Y_1 & \cdots & Y_{n_{good}} \\ 0 & \cdots & 0 & 1 & \cdots & 1 \\ -x_1X_1 & \cdots & -x_{n_{good}}X_{n_{good}} & -y_1X_1 & \cdots & -y_{n_{good}}X_{n_{good}} \\ -x_1Y_1 & \cdots & -x_{n_{good}}Y_{n_{good}} & -y_1Y_1 & \cdots & -y_{n_{good}}Y_{n_{good}} \end{bmatrix}^t, \tag{8}$$

b is $1\times 2n_{good}$ real matrix:

$$b = \begin{bmatrix} x_1 \ldots x_{n_{good}} y_1 \ldots y_{n_{good}} \end{bmatrix}, \tag{9}$$

and h is also 1×8 real matrix:

$$h = \begin{bmatrix} h_{11} & h_{12} & h_{13} & h_{21} & h_{22} & h_{23} & h_{31} & h_{32} \end{bmatrix}. \tag{10}$$

In theory, only four pairs of points (P_i,p_i), $i=1,2,\ldots,n$, $n_{good}=4$ are needed to obtain values of h_{ij}. Practically, number of "good" points should be much higher in order to obtain high accuracy of results, e.g. more than 50 for total number of calibration points about 2000.

The most popular method, which serves solving least square method is using the pseudoinverse matrix A^+ [12]. It uses SVD computation. However, size of A depends linearly on number of "good" points and for large number of them time complexity can become a problem. Therefore, for large number of points we propose to reformulate equations.

Equations (4) means that:

$$p = \lambda_p HP, \quad \lambda_p \in R. \tag{11}$$

We use the hat operation, which implements the vector product with p:

$$\hat{p} = \begin{bmatrix} 0 & -1 & y \\ 1 & 0 & -x \\ -y & x & 0 \end{bmatrix}. \tag{12}$$

Both sides of equation (11) can be multiplied by $\hat{p}$:

$$\hat{p}p = \lambda_p \hat{p}HP. \tag{13}$$

Notice that $\hat{p}p = 0_{3\times1}$. After dividing both side of (13) by λ_p it is obtained:

$$\hat{p}HP = 0. \tag{14}$$

Product HP can be written as:

$$HP = \begin{bmatrix} h_1^tP \\ h_2^tP \\ h_3^tP \end{bmatrix} = \begin{bmatrix} P^th_1 \\ P^th_2 \\ P^th_3 \end{bmatrix} = \begin{bmatrix} P^t & 0_{1\times3} & 0_{1\times3} \\ 0_{1\times3} & P^t & 0_{1\times3} \\ 0_{1\times3} & 0_{1\times3} & P^t \end{bmatrix} \begin{bmatrix} h_1 \\ h_2 \\ h_3 \end{bmatrix}. \tag{15}$$

A product of two matrices is obtained. First of the matrix is Kronecker's product of identity matrix $I_{3\times3}$ and P^t. The second one is column vector consisted of sought elements of homographic matrix H:

$$HP = (I_3 \otimes P^t)vec(H). \tag{16}$$

Inserting (16) into (14):

$$\underbrace{\hat{p}(I_3 \otimes P^t)}_{A}\underbrace{vec(H)}_{x} = 0. \tag{17}$$

We can write such equation for all "good" calibration points:

$$\underbrace{(\hat{p}_i \otimes P_i^t)}_{A_i}\underbrace{vec(H)}_{x} = 0, \quad i = 1, \cdots, n_{good}. \tag{18}$$

We obtained a set of linear equations, which can be solved using the least square method. However, in order to avoid solution $x=0_{8\times1}$, we consider the quadratic form:

$$x^tA^tAx = 0. \tag{19}$$

For all "good" calibration points it holds:

$$x^t\left(\sum_{i=1}^{n_{good}} A_i^tA_i\right)x = 0, \tag{20}$$

where the expression in brackets we call as the secondary matrix B:

$$B = \sum_{i=1}^{n_{good}} A_i^tA_i, \tag{21}$$

instead of matrix (8) which is called as the primary matrix.

Because matrix B is symmetric and semidefinite, EVD decomposition of this matrix produce the same results as SVD. This property can be used to determine the solution of (20), which is the eigenvector corresponding to the smallest singular value. It means that having $SVD(B)=U\Sigma V^t$, the solution for $vec(h)$ is the last column of U.

2.3.2 Distortion Centre Estimation

Point $p \equiv HP$ is the image of P, which is then distorted along the direction of $p\text{-}p_0$. Therefore, points p_0, p, $\tilde{p}$ are collinear and the following matrix is singular:

$$\det\left[p - p_0, \tilde{p} - p_0\right] = 0. \tag{22}$$

For every calibration point which is distorted significantly (called "bad" point) the equation (22) is true:

$$\det[p_i - p_{0,} \tilde{p}_i - p_0] = 0, \quad i = 1 + n_{good}, ..., n. \tag{23}$$

Having a set of such equations, the solution for distortion centre p_0 can be obtained by LSM.

2.3.3 Radial Coefficients Estimation

Having the homographic matrix H and localised "good" points, undistorted pixel co-ordinates for "bad" points can be calculated. Differences between these estimated undistorted localisations and real distorted localisation of "bad" points have the models:

$$\begin{aligned} \tilde{x}_i' - x_i' &= d_1 x_i' r_i' + d_2 x_i' r_i'^2 + d_3 x_i' r_i'^3 + d_4 x_i' r_i'^4, \\ \tilde{y}_i' - y_i' &= d_1 y_i' r_i' + d_2 y_i' r_i'^2 + d_3 y_i' r_i'^3 + d_4 y_i' r_i'^4, \\ i &= 1, ..., n, \end{aligned} \tag{24}$$

where:

$$\begin{aligned} r_i' &= \| p_i - p_0 \|, \\ x_i' &= x_i - x_0, \quad \tilde{x}_i' = \tilde{x}_i - x_0, \\ y_i' &= y_i - y_0, \quad \tilde{y}_i' = \tilde{y}_i - y_0. \end{aligned} \tag{25}$$

The distortion parameters are found using LSM iteratively selecting the number of "good points".

2.4 Distortion compensation

For the whole image compensation, we consider the target image as the one which is distorted and therefore the unknown colour of target pixel can be found by applying the radial distortion model to coordinates of target pixel and next filtering colours in the distorted image around the obtained source pixel. The required colour is obtained by the bilinear interpolation of four nearest pixels of the source. This simple approach gives satisfactory results.

3. EXPERIMENTS

The presented system was tested on images acquired by following digital devices: camcorder SONY EVI-D31, two cameras Olympus C-7070 and camera SONY DSC-S600. Experiments showed, that calibration points can be localised with subpixel accuracy (exemplary results are shown in Fig. 2a-c).

Tests showed also that values of distortion parameters estimated by the method leads to obtain subpixel accuracy of image correction. As quality measure the deviation from the best fitted straight lines were used. The lines were found using PCA analysis. Exemplary compensated image is shown in Fig. 2d.

The deviation of compensated points for different number of "good" points is presented in Fig. 3-4 (total

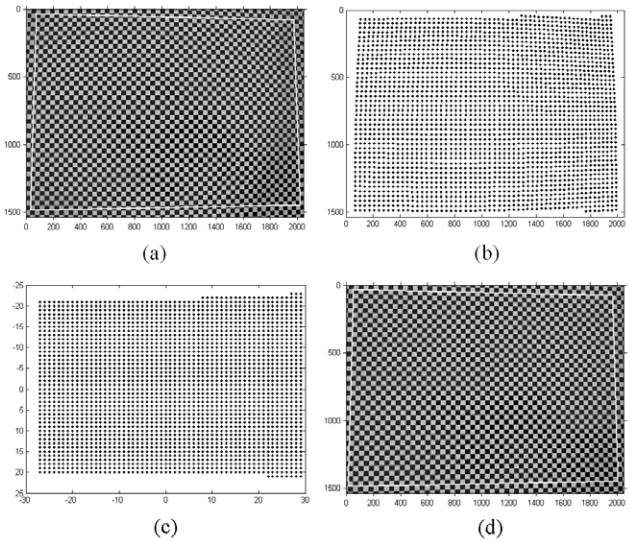

Figure 2 – Exemplary results for camera SONY DSC-S600: (a) – original image with straight lines added, (b) – localised calibration points, (c) – indexes of calibration points, (d) – compensated image with straight lines added

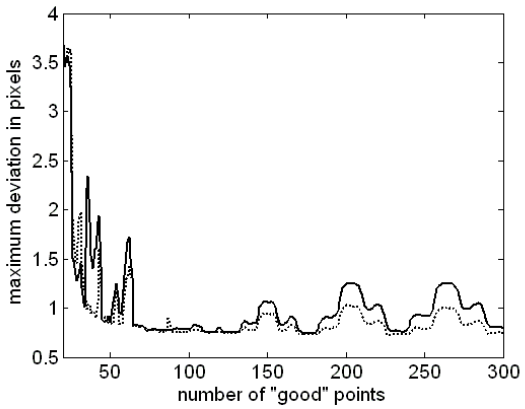

Figure 3 – Maximum deviation of compensated points from straight lines for method using primary matrix (solid line) and secondary matrix (dotted line) for homographic matrix computation

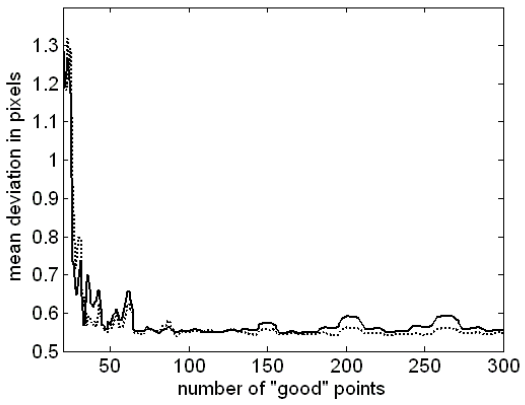

Figure 4 – Mean deviation of compensated points from straight lines for method using primary matrix (solid line) and secondary matrix (dotted line) for homographic matrix computation

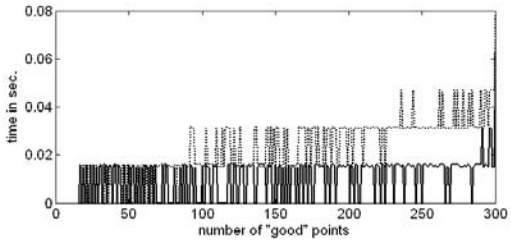

Figure 5 – Exemplary executing time for implementations with primary matrix (solid line) and secondary matrix (dotted line) for homographic matrix computation

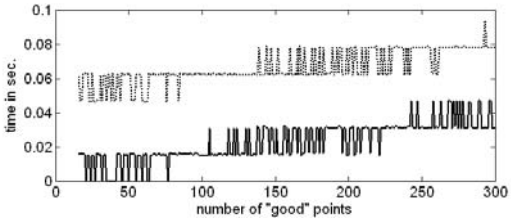

Figure 6 – Exemplary executing time for implementations with primary matrix (down) and secondary matrix (up) for radial parameters estimation

number of detected calibration points is about 2400). For primary matrix method used for homographic matrix estimtation optimal number of "good" points is 177, for this number maximum deviation is about 0.742 pixel.

The approaches of the primary and the secondary matrix were tested by the least square method for homographic matrix estimation and radial parameters estimation. Method using secondary matrix usually provides slightly better estimation of homographic matrix (Fig. 3-4). For the radial parameters estimation differences between obtained values of the parameters were negligible, while the executing time was better for solution using primary matrix (Fig. 6).

Using compensation model instead of distortion model does not improves the results. For the example illustrated above the maximum deviation is about 0.769 pixel for optimal number of "good" points equal to 171 for primary matrix method using the following compensation model (cf. (1)):

$$p = d(\tilde{p}) = p_0 + (\tilde{p} - p_0)[1 + d_1 \| \tilde{p} - p_0 \| + d_2 \| \tilde{p} - p_0 \|^2 + d_3 \| \tilde{p} - p_0 \|^3 + d_4 \| \tilde{p} - p_0 \|^4]. \quad (26)$$

4. CONCLUSION

A novel method for extracting distorted grid points for compensation of lens radial nonlinearities is presented. It is based on identification of homographic transformation using single image of dense planar chessboard pattern. Undistorted grid image is determined from the central part of the grid and used to find the radial distortion model by linear least square method (LSM). The algorithm includes steps for fast localisation of calibration points using designed neighbourhood analysis instead of more complex popular techniques like Harris filters for corner detection.

Two versions of least square method were tested for homographic matrix estimation and for values of distortion parameters estimation. Primary matrix method needs computation of SVD on bigger matrices than secondary matrix method. However, the second method is generally more time consuming because of complex data preparation process for SVD computation. Nevertheless, use of secondary matrix method for homographic matrix estimation increases slightly the accuracy of results.

ACKNOWLEDGEMENT

The work presented was developed within VISNET 2, a European Network of Excellence (http;//www.visnet-noe.org), funded under the European Commission IST FP6 Programme.

REFERENCES

[1] D.C. Brown, "Decentering distortion of Lenses," *Photometric Engineering*, vol. 32, no. 3, pp. 444–462, 1966.
[2] F. Devernay, O. Faugeras, "Straight lines have to be straight," *Machine Vision and Application*, vol. 13, no. 1, pp. 14-24, 2001.
[3] R.Y. Tsai, "A versatile camera calibration technique for high-accuracy 3D machine vision metrology using off-the-shelf TV cameras and lenses," *IEEE J. of Robot.. and Aut.*, 3, pp. 323-244, 1987.
[4] Z. Zhang, "Flexible camera calibration by viewing a plane from unknown orientation," *IEEE International Conference on Computer Vision*, pp. 666-673, Sep. 1999.
[5] H.S. Sawhney, R. Kumar, "True multi-image alignment and its application to mosaicing and lens distortion correction," *IEEE Trans PAMI*, 14, no. 3, pp. 235-243, 1999.
[6] G.P. Stein, "Lens distortion calibration using point correspondence," *Proc. CVPR*, pp. 602-608, 1997.
[7] J. Heikkila, "Geometric camera calibration using circular control points," *IEEE Trans. on Pattern Anal. and Mach. Int.*, vol. 22, no. 10, pp. 1066-1077, Oct. 2000.
[8] Ch. Braüer-Burchardt, K. Voss, "Automatic lens distortion calibration using single views," pandora.inf.uni-jena.de/papers/calibration.ps.
[9] D.C. Brown, "Close range camera calibration," *Photogrammetric Engineering*, vol. 37, no. 8, pp. 855-866, 1971.
[10] S.B. Kang, "Radial distortion snakes," *IEICE Trans. Inf. & Syst.*, vol. E84-D, no. 12, pp. 1603-1611, Dec. 2001.
[11] H. Farid, A.C. Popescu, "Blind removal of lens distortion," *Journal of the Optical Society of America A, Optics, Image Science, and Vision*, vol. 18, no. 9, pp. 2072-2078, Sep. 2001.
[12] R. Klette, K. Schluus, A. Koschan, *Computer Vision. Three-Dimensional Data from Images*, Springer-Verlag Singapore Pte. Ltd., 1996.
[13] J. Canny, "A computational approach to edge detection," *IEEE Trans. Pattern Anal. and Mach. Int.*, vol. 8, no. 6, pp. 679-698 Nov. 1986.
[14] A. Nowakowski, W. Skarbek, "Fast computation of thresholding hysteresis for edge detection," in *Proc. of SPIE Volume 6159: Photonics Appl. in Astrn., Comm., Industry, and High-Energy Physics Exp. IV*, 61593D, Feb. 2006.
[15] A. Nowakowski, M. Tomaszewski, "Chessboard Pattern Reconstruction for Camera Calibration System," in *Proc. National Conf. on Radiocommunications and Broadcasting KKRRiT* 2005, *Special VISNET Session*, Kraków, Poland, June 17, 2005, pp. 7-10.
[16] I.T. Jolliffe, *Principal Component Analysis*, Second Edition, Springer-Verlag New York Inc., 2002.
[17] G.H. Golub, Ch.F. van Loan, *Matrix Computations*, Second Edition, The Johns Hopkins University Press, 1989.